Am J Transl Res 2023;15(4):2370-2388
www.ajtr.org /ISSN:1943-8141/AJTR0146299

Original Article

TSF/FHA induces osteogenic differentiation of Mc3t3 cells via Pygo2 dependent Wnt/β-catenin signaling pathway

Wenhang Dong[1,2], Rui Li[1], Minglei Sun[1], Hongyan Mi[1,3], Meiyue Wang[1,3], Mengzhe Liu[1,3], Weiliu Qiu[1,3,4]

[1]Department of Stomatology, The First Affiliated Hospital of Zhengzhou University, Zhengzhou, Henan, China; [2]Academy of Medical Sciences at Zhengzhou University, Zhengzhou, Henan, China; [3]Department of Oral and Maxillofacial Surgery, Ninth People's Hospital, School of Medicine, Shanghai Jiao Tong University, Shanghai, China; [4]Shanghai Key Laboratory of Stomatology, Shanghai, China

Received September 2, 2022; Accepted December 16, 2022; Epub April 15, 2023; Published April 30, 2023

Abstract: Objectives: This study aimed to investigate whether tussah silk fibroin (TSF)/fluoridated hydroxyapatite (FHA) can promote osteogenic differentiation of Mc3t3 cells and explore the role of Wnt/β-catenin signaling in this process. Methods: TSF/FHA was gained via freeze drying technique and cyclic phosphate immersion method. The relative expression levels of bone-related genes and proteins of Mc3t3 cells seeded on different materials were examined by RT-qPCR and Western blotting. Knockdown or overexpression of Pygo2 in Mc3t3 cells was achieved using lentiviral transfection. Cell proliferation, the expression of bone-related genes and proteins were subsequently examined. Animal experiment was also performed to observe the osteogenesis effect. Results: Different ratios of fluorine of TSF/FHA accelerated the osteogenic differentiation of Mc3t3 cells and increased the Pygo2 expression. The Wnt/β-catenin signaling pathway was activated after TSF/FHA induction, accompanied by the increased expression of related genes. In SD rats with skull defect, the newly formed bone increased significantly and the Pygo2 overexpressing Mc3t3 cells promoted osteogenesis. However, Pygo2 knockdown markedly compromised the osteogenesis of Mc3t3 cells after TSF/FHA induction. Conclusion: TSF/FHA facilitates osteogenic differentiation of Mc3t3 cells via upregulating Pygo2 and activating Wnt/β-catenin signaling pathway.

Keywords: Silk fibroin, fluoro-hydroxyapatite, fluorapatite and hydroxyapatite, Mc3t3, osteogenesis

Introduction

Bone defects caused by trauma, tumor or congenital dysplasia are very common and may affect the configuration and function of human bones [1, 2]. The development of materials for the bone repair has been a hot topic in the orthopedic field. The materials used for artificial replacement can be divided into three types: (1) synthetic biomolecular materials such as polylactic acid (PLA), polyglycolide (PGA) and polyglycolide-polylactic acid (PGA-PLA) copolymer [3, 4]: the degradation products of these materials are acidic *in vivo* and *in vitro*, and the adhesion of cells to these materials is weak, which is not conducive to cell growth and passage [5]; (2) synthetic inorganic materials such as HA and tricalcium phosphate (TCP) compounds [6]: their degradation time is difficult to control, and they have relatively high brittleness, and thus they are not applicable in the dynamic reconstruction of new bone [7]; (3) derived materials of natural organisms: they are easy to degrade [8], and usually not used for osteogenesis alone.

In recent years, a variety of composite scaffolds have been developed. Silk fibroin/hydroxyapatite (SF/HA) as a tissue engineering composite scaffold that has been studied for many years, and the characteristics of SF and HA have been deeply discussed [9]. SF is a natural polymer protein [10], and has abundant raw materials, good biocompatibility, non-toxic degradation products and low immunogenicity [11]. Biomaterials such as SF microspheres, SF membranes and SF sponges can be obtained through different technical processes [12]. The

biomedical materials currently under use include drug sustained-release materials, biosensors, surgical sutures, tissue-engineered scaffolds and so on [12]. The content of silk protein in tussah silk fibroin (TSF) is higher than that in the mulberry silk, and the natural arginine-glycine-aspartic acid (Arg-Gly-Asp) tripeptide structure of TSF can promote the osteoblast adhesion, cell-cell interaction and tissue regeneration in the bone, cartilage and nerve regeneration [12, 13]. Therefore, TSF was used to mimic the organic component in the natural bone in our study. Although hydroxyapatite can promote the adhesion of osteoblasts and has good bone conduction and bone induction activities [14], it doesn't provide a friendly surface for cells [15]. Studies about fluoridated hydroxyapatite (FHA) have been reported that moderate fluoride ions substituting hydroxyl groups have higher crystallinity and better biological activity [16]. Therefore, FHA was used in this study as the inorganic components of natural bone. In other words, TSF and FHA mimic the organic and inorganic components of natural bone respectively. However, whether TSF/FHA is able to induce osteogenesis and the specific mechanism remain unclear.

Mc3t3 cells are mouse precranial cells [17] and can undergo osteogenic differentiation under certain induction conditions [18]. The process of osteogenic differentiation of Mc3t3 cells requires the precise control of the Wnt/β-catenin signaling pathway, an important pathway which has been reported to regulate several regenerative processes [19, 20]. Pygo2 is a very important positive factor of the Wnt/β-catenin pathway [21]. When β-catenin accumulates in the cytoplasm, it enters the nucleus and Pygo2 directly binds to the Legless which then binds to β-catenin [21]. Thus, the transcription of downstream target genes of Wnt/β-catenin signaling pathway is enhanced, and the adipogenesis is negatively regulated [22]. However, the exact role of Wnt/β-catenin signaling pathway in the osteogenic differentiation of Mc3t3 cells induced by TSF/FHA remains unknown. Moreover, little is known about the influence of Pygo2 on the osteogenesis. This study aimed to investigate the influence of TSF/FHA on the osteogenic differentiation of Mc3t3 cells, especially the role of Pygo2. We speculated that TSF/FHA might induce the Pgyo2 expression to activate Wnt/β-catenin signaling pathway and then promote the osteogenic differentiation of Mc3t3 cells.

Materials and methods

Ethics approval

The study was approved by the Medical Ethics Committee of the First Affiliated Hospital of Zhengzhou University and was funded by grants from the Oral and Maxillofacial Surgery Academician Workstation of Zhengzhou (152PYSGZ040).

TSF/FHA fabrication

Tussah cocoons were purchased from Nanyang in Henan Province, China. All chemicals of analytical grades were commercially purchased in China. To remove the sericin, cocoons was degummed with 0.5% Na_2CO_3 solution at 100°C thrice. Degummed tussah fiber was dissolved in 9 M aqueous lithium thiocyanate solution at a liquor ratio of 10:1 by stirring at 55°C for 1 h. Then the TSF aqueous solution was filtered to remove undissolved part, and dialyzed for 3 days in deionized water using a cellulose dialysis membrane with cut off molecular weight of 8-14 kDa. The pure TSF solution was finally obtained. After 24 h, the spongy TSF was obtained in a freeze dryer at -80°C and sealed at -20°C.

Then, 0.8 g of TSF was dissolved in 10 ml of hexafluoroisopropanol (HFIP), and the mixture was stirred on a magnetic agitator for 1 day. After TSF was completely dissolved, the TSF solution was added into a 10-ml syringe. TSF electrostatic spinning film was obtained with a propulsion speed at 1.5 ml/h and a voltage at 24 KV. The distance between the needle tip of the syringe and the receiving device was 15 cm, and the speed of receiving drum was 2000 rpm. The conformation of SF and its infrared spectral wavenumber range were shown in Supplementary Table 1.

Coating of F_XHA on TSF nanofiber surfaces

The synthesis and coating of F_XHA crystals on the TSH nanofiber scaffolds were performed using previously reported method [23, 24] with modification. For a typical synthesis of F_XHA crystals, the scaffolds were treated with 0.2 M $CaCl_2$ for 12 h, then 0.12 M $(NH4)_2HPO_4$, and NH_4F at different concentrations (0 M, 0.02 M, 0.04 M) at 37°C under ambient pressure for 12 h. These procedures were repeated thrice. $NH_3{\cdot}H_2O$ was used to adjust the pH to >7.0. The

final materials were TSF/F_0HA, TSF/F_1HA and TSF/F_2HA. The final scaffolds with F_XHA layer were rinsed with PBS and then dried in air. Scanning electron microscope (SEM), energy dispersive spectroscopy (EDS), fourier transform infrared spectroscopy (FTIR) and X-ray diffraction (XRD) were used to identify the TSF, TSF/F_0HA, TSF/F_1HA and TSF/F_2HA.

Cell culture and seeding

Mc3t3 cells were purchased from Chinese Academy of Science and maintained in complete medium under standard culture conditions. The medium was refreshed once every 2-3 days, and cells of passages 3-5 were used in the following experiments.

Before cell seeding, 4 kinds of scaffolds with F_XHA (TSF/F_XHA) or without FHA (TSF) were cut into 1.0 cm^2 ones and then placed into the 48-well plates. Both sides of each scaffold were sterilized for 1 h and then incubated with Penicillin-Streptomycin solution for 2 h and in complete medium overnight before using.

Mc3t3 cells of the third passage were seeded into 48-well plates with scaffolds at a density of 1 × 10^4/ml cells per scaffold. The medium was refreshed once every 2-3 days. Cell morphology was observed under SEM. The cell proliferation was detected by EdU staining and CCK-8 assay, and the expression of osteogenesis related genes and proteins by qRT-PCR and Western blotting, repectively. The experiments were repeated thrice.

Alizarin red and alkaline phosphatase (ALP) stainings

In order to study the effects of different scaffold materials on the osteogenic differentiation of Mc3t3 cells, cells were grown in complete medium with/without different materials. The medium was refreshed once every 2-3 days. After 7-day culture, cells were subjected to ALP staining. After 21-day culture, cells were processed for alizarin red staining.

Lentiviral transduction

Lentiviral particles (Gene Chen, Shanghai, China) were used to construct Pygo2 overexpressing (LV-Pygo2) or knockdown (LV-sh-Pygo2) cells. Transduction with lentiviral particles encoding scrambled sequences served as a negative control (Sh-NC or LV-NC). The infection multiplicity (MOI) was 50, and the transfection efficiency was over 70%. After transfection for 6 h, cells were transferred to complete medium. When the cell confluency reached 80%, cells were screened with 3 μg/mL puromycin and untreated cells served as a control.

RNA isolation and qRT-PCR

Trizol was used to extract RNA from Mc3t3 cells followed by cDNA synthesis using the Prime Script RT kit (Takara, Shiga, Japan) according to the manufacturer's instructions. cDNA was then amplified by qRT-PCR using the SYBR Premix Ex Taq™ II kit (Takara, Shiga, Japan) on a Fast Dx Real-Time PCR instrument (Applied Biosystems 7500, USA) with following conditions: 95°C for 30 s, 45 cycles of 95°C for 5 s, 60°C for 34 s, 95°C for 15 s, 60°C for 1 min and 95°C for 15 s. The gene expression was determined using the $2^{-\Delta\Delta CT}$ method; GAPDH served as an internal control. All experiment were repeated thrice.

RNA sequencing

RNA-sequencing (RNA-seq) was performed in 6 samples (n=3 in control group; n=3 in TSF/FHA group). First, total RNA was extracted and reversely transcribed into double-stranded cDNA [25].

The sequencing data were filtered with SOAP nuke (v1.5.2) by the following steps: (1) reads of the adapter sequences were removed; (2) low-quality reads (base quality less than or equal to 20) were removed; (3) reads with an unknown base ('N' base) ratio higher than 5% were removed. Differentially expressed genes were those with a False Discovery Rate (FDR) ≤0.001 and a |Log2Ratio| >1. Additionally, GO (http://www.geneontology.org/) and KEGG (https://www.kegg.jp/) enrichment analyses were performed using Phyper (https://en.wikipedia.org/wiki/Hypergeometric_distribution) based on the Hypergeometric test. The significant levels of terms and pathways were corrected using Q value with a rigorous threshold (Q value ≤0.05) as per the Bonferroni test.

Western blotting

Total protein (20 μg) was extracted from each sample, separated on 10% SDS-PAGE and subsequently transferred onto polyvinyl difluoride

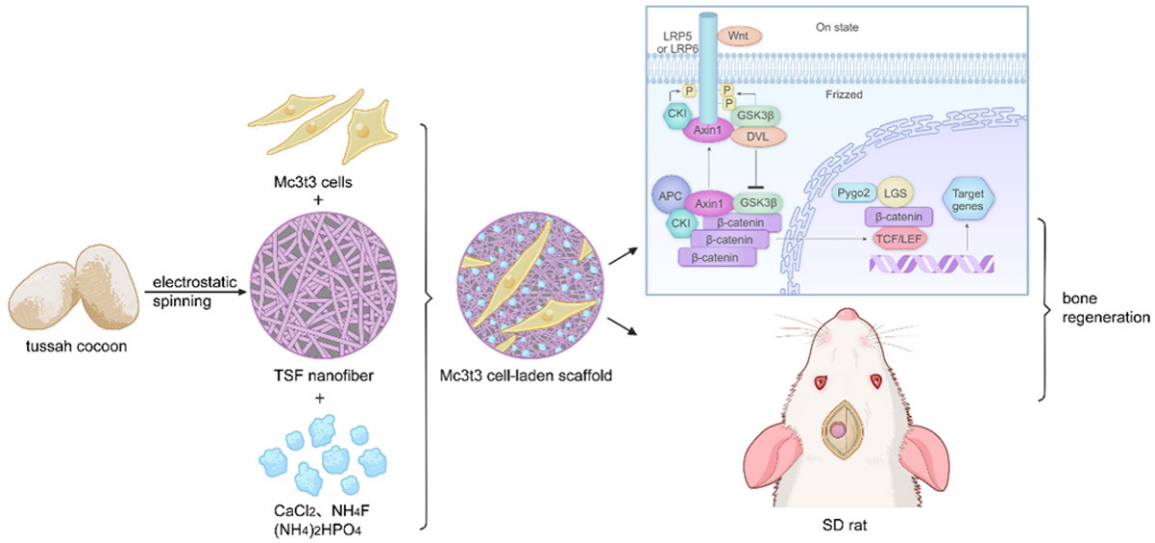

Figure 1. Schematic diagram of Mc3t3 cells cultured with TSF/FHA for bone regeneration. Tussah Silk Fibroin (TSF)/Fluoridated Hydroxyapatite (FHA).

(PVDF) membranes (Millipore, USA). The membranes were blocked with 5% bovine serum albumin (BSA) for 2 h at room temperature, and then incubated with primary antibodies (1:1000), including RUNX2 (Abcam), ALP (Thermo), OPN (Abcam), OCN (Affinity), BSP (Thermo), COL-1 (Abcam) and GAPDH (1:10000, Abcam) overnight at 4°C. To detect β-catenin, Mc3t3 cells were stimulated with primary antibodies (1:1000) against Pygo2, active β-catenin and β-catenin.

After washing with TBST thrice, membranes were incubated with secondary antibodies (horseradish peroxidase-conjugated goat anti-rabbit or anti-mouse IgG, 1:10000, Jackson) at room temperature for 2 h. The proteins were visualized with a GE Amersham Imager 600 instrument (USA). This assay was repeated thrice for each protein. Then, ImageJ software (National Institutes of Health, USA) was used to analyze the gray value.

Bone regeneration experiment in SD rats

SD rats aged 6-7 weeks were purchased from Beijing Victory and randomly divided into 5 groups: Group A (control), Group B (TSF/FHA), Group C (TSF/FHA + untreated Mc3t3 cells), Group D (TSF/FHA + LV-Pygo2 Mc3t3 cells), Group E (TSF/FHA + LV-sh-Pygo2 Mc3t3 cells). Cells in the B-E groups were incubated on the TSF/FHA at 37°C for 5 days. After deep anesthesia, cells in the B-E groups with TSF/FHA and cells in the A group were implanted on the 5-mm skull defect site of SD rats. After 8 weeks, the skulls were harvested from these rats, fixed in 4% paraformaldehyde overnight, and subjected to micro-CT imaging and μCT reconstruction. Then, the skulls were embedded in paraffin and sliced. The sliced sections were subjected to hematoxylin and eosin staining, Masson staing and immunohistochemical staining. All animal experiments were carried out in accordance with the guidelines of Animal Experiment Committee of Zhengzhou University. The guidelines are also in line with the Care and Use of Laboratory Animals of the National Health Research Institute of Zhengzhou University. **Figure 1** shows the strategy of Mc3t3 cells cultured with TSF/FHA for bone regeneration.

Statistical analysis

Statistical analysis was performed with SPSS version 21.0 software (USA). T-test, corrected t-test and one-way analysis of variance were used for the comparisons of data among groups. A value of $P<0.05$ was considered statistically significant.

Results

Characteristics of materials in four groups

TSF and TSF/F_XHA are composed with Ca, P and F at different ratios and were constructed in this experiment. Scanning electron micros-

copy showed that the materials in four groups contained continuous nanofibers, but there was no significant difference in the diameter (**Figure 2**). Before the preparation of composite scaffolds by phosphate cycling immersion method, the average diameter of nanofiber in four groups was 194.3 nm, 199.6 nm, 189.2 nm and 190.2 nm, respectively (**Figure 2B**). There was no significant difference in the TSF fiber diameter among four groups (P>0.05).

There were bubble-like structures between fibers, which might be ascribed to the slightly high concentration of spinning solution. The TSF film surface of TSF/F_XHA was deposited by the inorganic crystals with relatively uniform distribution (**Figure 2A**).

FTIR (**Figure 3A**) showed that the absorption peaks of materials in 4 groups were observed at 675 cm^{-1}, 1261 cm^{-1}, 1517 cm^{-1} and 1653 cm^{-1}, respectively and the peak at 1653 cm^{-1} was the highest. These absorption peaks corresponded to the random crimping of TSF amide IV, β folding of amide III, β folding of amide II and characteristic absorption peaks of α helix of amide I, respectively. As shown in Supplementary Table 1, the prepared nanofilm was TSF film and its main structure was α helix of amide I. The two absorption peaks of phosphoric acid root were located at 960 cm^{-1} and 1050 cm^{-1}, respectively, and the asymmetric stretching vibration peak of hydroxyl group was located at 3562 cm^{-1}. These absorption peaks were absent on the TSF film, indicating that there was no HA deposition on the surface of materials in this group. The composite materials in remaining three groups all had two absorption peaks of phosphoric acid, and TSF/F_0HA and TSF/F_1HA had the absorption peaks of hydroxyl at 3562 cm^{-1}, indicating that the materials in these two groups contained hydroxyapatite. The absorption peak of TSF/F_1HA in this study was weaker than that of TSF/F_0HA, indicating that the number of hydroxyl groups in the TSF/F_1HA reduced after being replaced by fluoride ions, while the absorption peak of TSF/F_2HA near 3562 cm^{-1} was very small, indicating that fluoride ions had a high degree of substitution for hydroxyl groups in the crystals of this group.

Studies have found that, compared with HA, FHA has a higher crystallinity and a more compact crystal structure [26]. XRD showed that the diffraction peaks of 002, 211 and 222 crystal planes in the TSF/F_1HA and TSF/F_2HA became increasingly sharp (**Figure 3B**), and 211 crystal plane was differentiated into two peaks, indicating that the crystallinity of 002 and 211 crystal planes increased with the increase of fluorine doping rate [27]. Among them, the largest difference of peak and valley between the 211 and 300 crystal planes of F_1HA meant that this group had the highest crystallinity. There was no obvious diffraction peak in the TSF, indicating that there was no crystal deposition on the surface of the material, which might be related to the short stretching processing of the droplet during the electrostatic spinning and the lack of conformational rearrangement of the molecules in the fiber and therefore it is difficult to form ordered crystals.

EDS indicated that TSF contained C, O and N elements and did not contain other mineralized crystal related elements, indicating that the material was organic and there was no inorganic deposition on the surface. TSF/F_0HA contained C, O, N, Ca, P and Na elements, and the Ca/P molar ratio was about 1.47, which was close to the Ca/P molar ratio of hydroxyapatite (1.67), indicating that hydroxyapatite is deposited on the surface of TSF film. The small amount of sodium element might be residual sodium ions in the processing of material. Both TSF/F_1HA and TSF/F_2HA contained C, O, N, Ca, P and F elements, and the Ca/P molar ratio in the TSF/F_1HA and TSF/F_2HA the was about 1.59 and 1.55, respectively, which were close to the Ca/P ratio of hydroxyapatite (1.67). The Ca/F molar ratio in the TSF/F_1HA and TSF/F_2HA was about 12.7 and 6.2, respectively, which were close to the Ca/F molar ratio of theoretical values (10 and 5), indicating that fluoro-hydroxyapatite was deposited on the surface of TSF films in the two groups, and the fluoride content in the TSF/F_2HA was higher than that in the TSF/F_1HA (**Figure 3C**).

Effects of different materials on the proliferation and osteogenic differentiation of Mc3t3 cells

Mc3t3 cells were incubated with 4 materials for 2 days. SEM showed that the cell morphology became more elongated and the cell orienta-

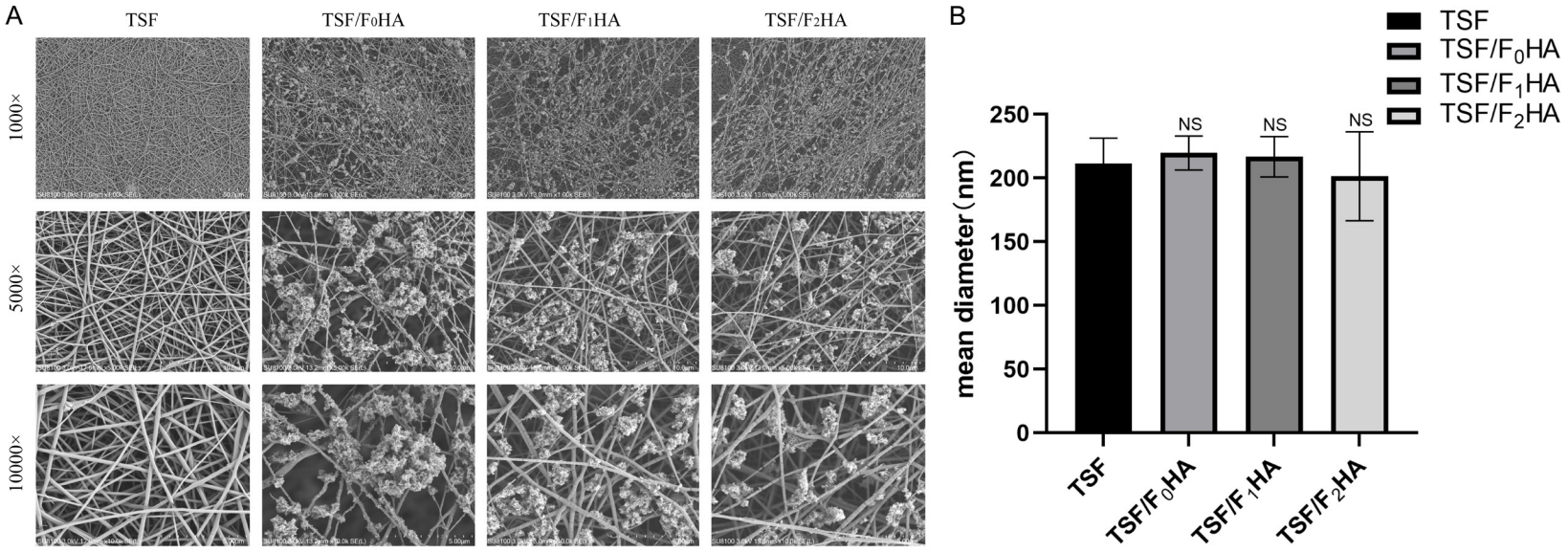

Figure 2. Average nanofiber diameter and SEM of TSF film and TSF/F_XHA with different Ca, P and F ratios. A. Before phosphate cycling immersion, the average nanofiber diameter was detected in 4 groups. B. SEM of inorganic crystals deposited on the surface of TSF film and TSF/FXHA with relatively unifo rm distribution. Scale bar is 50 μm (1000 ×), 10 μm (5000 ×) and 5 μm (10000 ×). Tussah Silk Fibroin (TSF)/Fluoridated Hydroxyapatite (FHA), Scanning Electron Microscope (SEM).

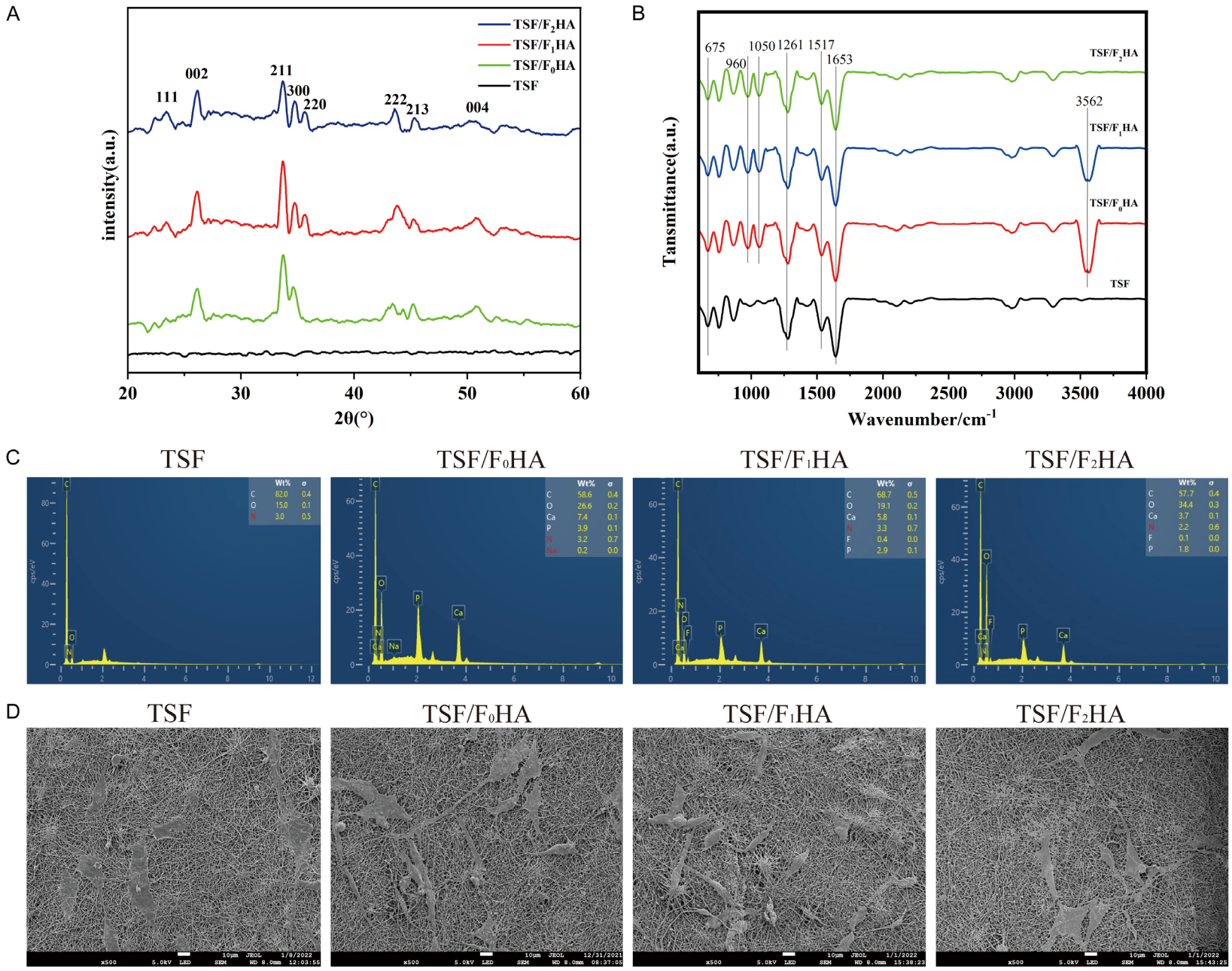
A
TSF/F2HA
TSF/F1HA
TSF/F0HA
TSF
002
211
111
300
220
222
213
004
intensity(a.u.)
20
30
40
50
60
2θ(°)
B
675
960
1050
1261
1517
1653
3562
TSF/F2HA
TSF/F1HA
TSF/F0HA
TSF
Tansmittance(a.u.)
1000
1500
2000
2500
3000
3500
4000
Wavenumber/cm-1
C
TSF
TSF/F0HA
TSF/F1HA
TSF/F2HA
D
TSF
TSF/F0HA
TSF/F1HA
TSF/F2HA

Figure 3. Charateristics of materials. A. FTIR of four materials. The absorption peaks of materials in 4 groups at 675 cm^{-1}, 1261 cm^{-1}, 1517 cm^{-1} and 1653 cm^{-1} were those of TSF film. Two absorption peaks of phosphoric acid root were located at 960 cm^{-1} and 1050 cm^{-1}, respectively and the asymmetric stretching vibration peak of hydroxyl group was located at 3562 cm^{-1}. B. XRD of four materials. The diffraction peaks of 002, 211 and 222 crystal planes in the TSF/F_1HA and TSF/F_2HA groups were sharper than those in the other two groups, and 211 crystal plane was differentiated into two peaks. There was the largest difference of peak and valley between 211 and 300 crystal planes of F_1HA rather than that in other groups. C. EDS of four materials. There was no inorganic deposition on the TSF film. Ca/P molar ratios was about 1.47, 1.59 and 1.55 in the TSF/F_0HA, TSF/F_1HA and TSF/F_2HA, respectively. Ca/F molar ratio was about 12.7 and 6.2 in the TSF/F_1HA and TSF/F_2HA, respectively. D. The morphology and orientation of Mc3t3 cells with four materials. Scale bar, 10 μm. Tussah Silk Fibroin(TSF)/Fluoridated Hydroxyapatite (FHA).

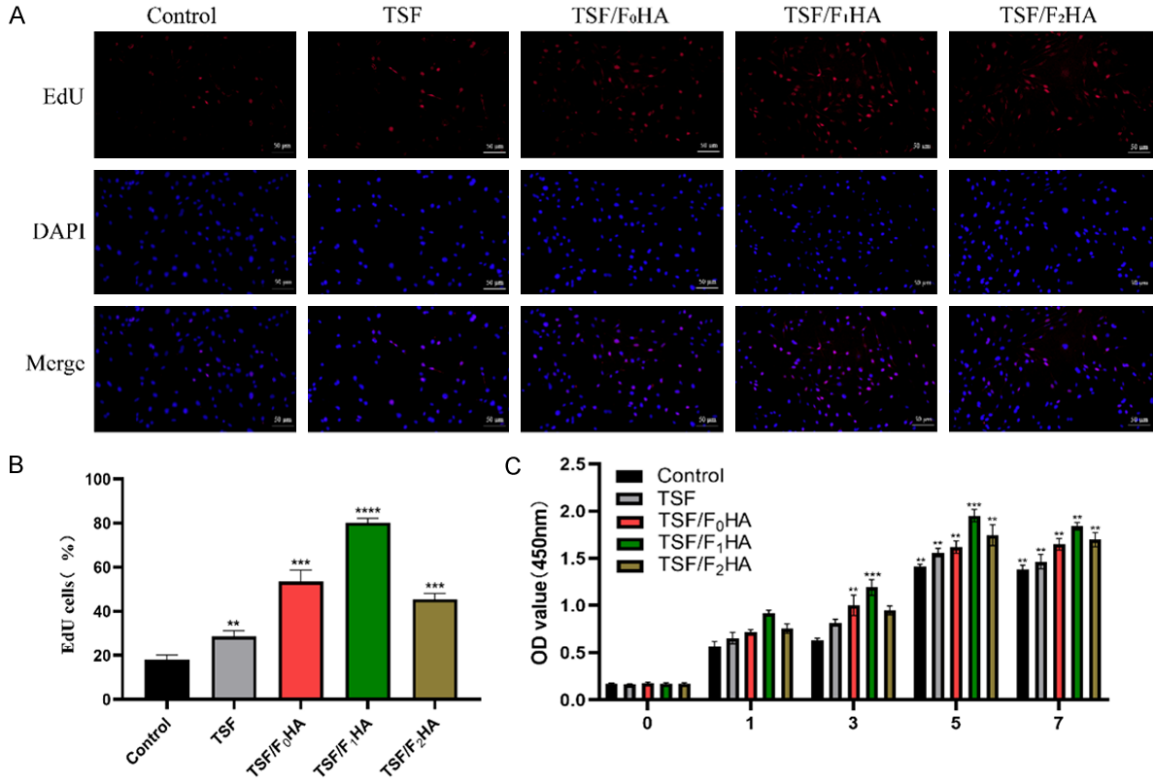

Figure 4. Effect of four materials on the proliferation of Mc3t3 cells. A, B. EdU staining showed that cells in the TSF/F_1HA group had the greatest proliferation rate. C. CCK-8 assay showed the same results in EdU staining. Scale bar, 50 μm. Tussah Silk Fibroin (TSF)/Fluoridated Hydroxyapatite (FHA).

tion was irregular (**Figure 3D**). There was no significant difference in the cell morphology among 4 groups. The effect of four materials on the proliferation of Mc3t3 cells was evaluated by EdU staining and CCK-8 assay. EdU staining indicated that the proportion of Mc3t3 cells in the proliferative phage in the TSF/F_1HA group was higher than that in the control group at 48 h, and TSF/F_1HA was the least cytotoxic (**Figure 4A**, **4B**). CCK-8 assay showed the cell proliferation rate in each group was similar to that in the control group on day 1. Moreover, the difference in cell proliferation rate increased over the next 5 days. Overall, TSF/F_1HA was the most beneficial to cell growth (**Figure 4C**).

To explore the effect of TSF/F_XHA on the osteogenic differentiation of Mc3t3 cells, alizarin red staining and ALP staining were conducted. All the scaffold materials showed deeper staining as compared to the control group, and the TSF/F_1HA group had the most calcium nodules and the deepest staining (**Figure 5A**, **5B**). Furthermore, the expression of genes and proteins related to osteogenesis was detected in these cells, including RUNX2, ALP, OPN, OCN, BSP and COL-1. The mRNA expression of these markers increased in all treated groups, with the highest expression in the TSF/F_1HA group (**Figure 5E**). In addition, the results of Western blotting were the same to those from qRT-PCR

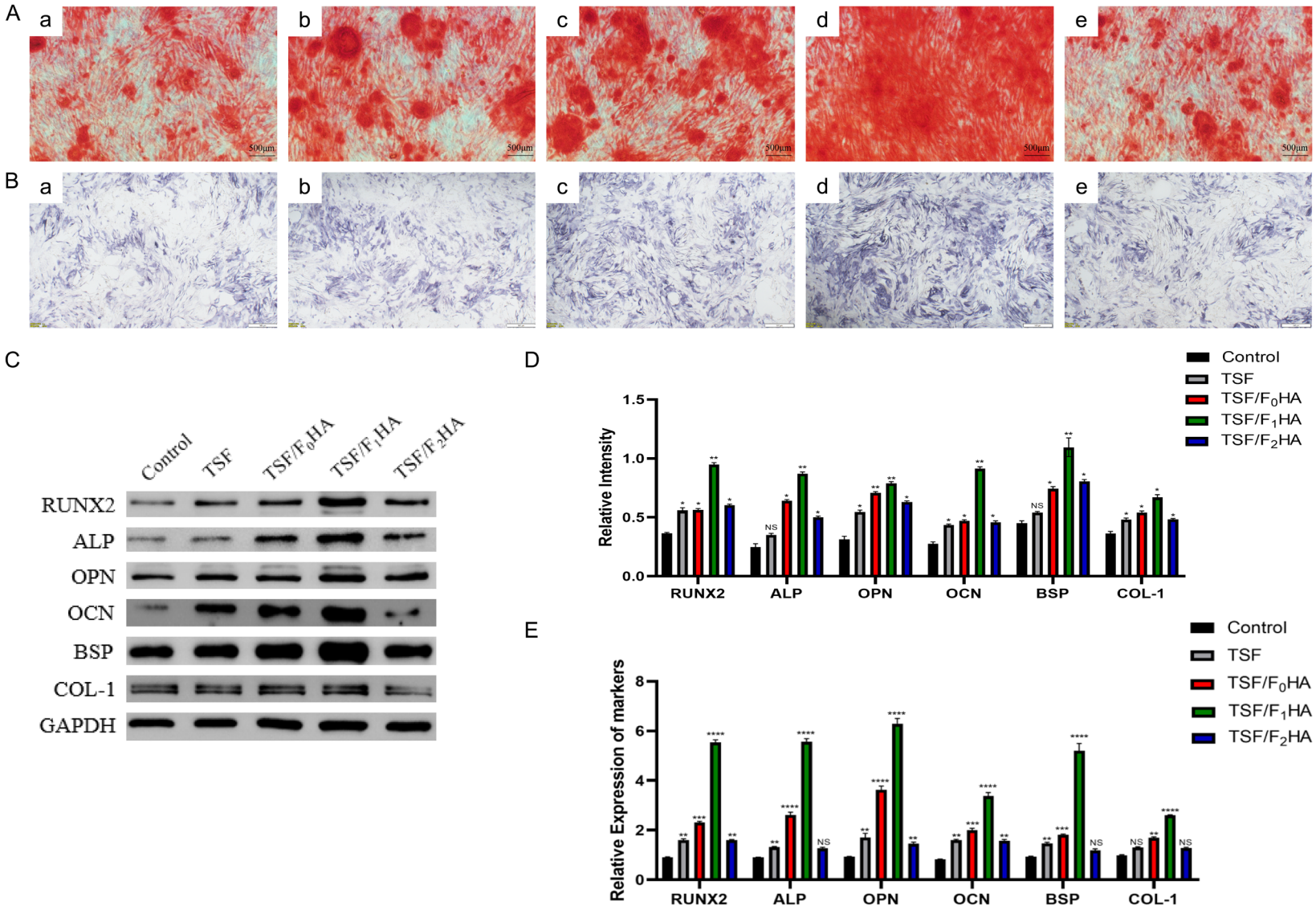

Figure 5. Effect of four materials on osteogenic differentiation of Mc3t3 cells. (A, B) The alizarin red and ALP stainings. (a) control, (b) TSF, (c) TSF/F_0HA, (d) TSF/F_1HA, (e) TSF/F_2HA. (C, D) Western blotting. (E) qRT-PCR. Scale bar, 50 μm (alizarin red staining) and 500 μm (ALP staining). Tussah Silk Fibroin (TSF)/Fluoridated Hydroxyapatite (FHA).

Table 1. Some differentially expressed genes between TSF/FHA induced- and control Mc3t3

Symbol	TSF/FHA	Control	log2 Fold Change
Ibsp	187.0704094	4.179406443	5.484139
Abca1	356.9787175	52.18458052	2.774143
Glul	1873.424476	320.2076522	2.548598
Angpt2	30.98318648	5.550446903	2.48081
Axin2	11.56652228	2.204021346	2.391745
Pygo2	312.63193334	24.05482722	3.700067
Col20a1	12.11283889	5.253231352	1.20526
Cd34	1759.918006	783.6812398	1.167169
Col27a1	903.8546911	414.3264308	1.125323
Irf9	20.71205347	9.928306605	1.060851
Lum	21.91494168	183.069705	-3.062406
Gbp4	1.04710046	8.78014066	-3.067844
Pgm5	2.217389403	21.13390455	-3.252625
Rasgrf1	1.213417166	12.21371868	-3.331355
Sema5a	21.46632895	222.1185588	-3.371183
Camk2a	1.005180154	10.66265544	-3.407041
Spry1	54.41069116	648.5701445	-3.575301
Kirrel3	13.40155776	162.396041	-3.599044
Cst6	5.75768556	86.23381148	-3.904693
Spon2	1.069079691	18.35048742	-4.101377

(**Figure 5C**, **5D**). Therefore, TSF/F_1HA was used in the following experiments and the name TSF/FHA was used for convenience.

TSF/FHA upregulates Pygo2 expression during the osteogenic differentiation of Mc3t3 cells

To further explore the mechanism underlying the TSF/FHA induced osteogenesis, RNA sequencing was employed to detect the gene expression in Mc3t3 cells of TSF/FHA group and control group. As compared to the control group, there were 1590 up-regulated genes and 636 down-regulated genes in the TSF/FHA group. The genes with significantly down-regulated or upregulated expression are listed in **Table 1** and **Figure 6A**, **6B**. The expression of Ibsp, Abca1, Axin2, Pygo2, Col20 a1 increased to different extents. Pygo2 is a positive regulator of Wnt/β-catenin signaling pathway and Axin2 is a target gene of this pathway. Our results showed Wnt/β-catenin signaling pathway was activated in Mc3t3 cells incubated with TSF/FHA. KEGG analysis was used to analyze the changes of pathways. The specific pathways are shown in **Table 2** and **Figure 6C**, **6D**. The Wnt/β-catenin signaling pathway was one of the most significantly altered pathways and thus this pathway was further investigated in the following experiments.

The gene and protein expression of Pygo2 were detected in cells of different groups. The Pygo2 expression increased in Mc3t3 cells during the TSF/FHA induced osteogenesis (**Figure 6E**, **6F**). These results suggest a relationship between the osteogenic differentiation and Pygo2 expression in the Mc3t3 cells incubated with TSF/FHA.

TSF/FHA regulated osteogenic differentiation of Mc3t3 cells via inducing Pygo2 expression

To further investigate the role of Pygo2 in TSF/FHA induced osteogenic differentiation of Mc3t3 cells, cells with Pygo2 knockdown or overexpression were generated. The transfection efficiency was assessed by qRT-PCR (**Figure 7C**). Since Pygo2 expression increased in the Mc3t3 cells treated with TSF/FHA as compared to control cells (**Figure 6E**, **6F**), LV-sh-Pygo2 and Sh-NC Mc3t3 cells were grown with TSF/FHA to determine the proliferation and osteogenic activites of Mc3t3 cells. Results showed the proliferation and expression of osteogenic genes and proteins decreased in

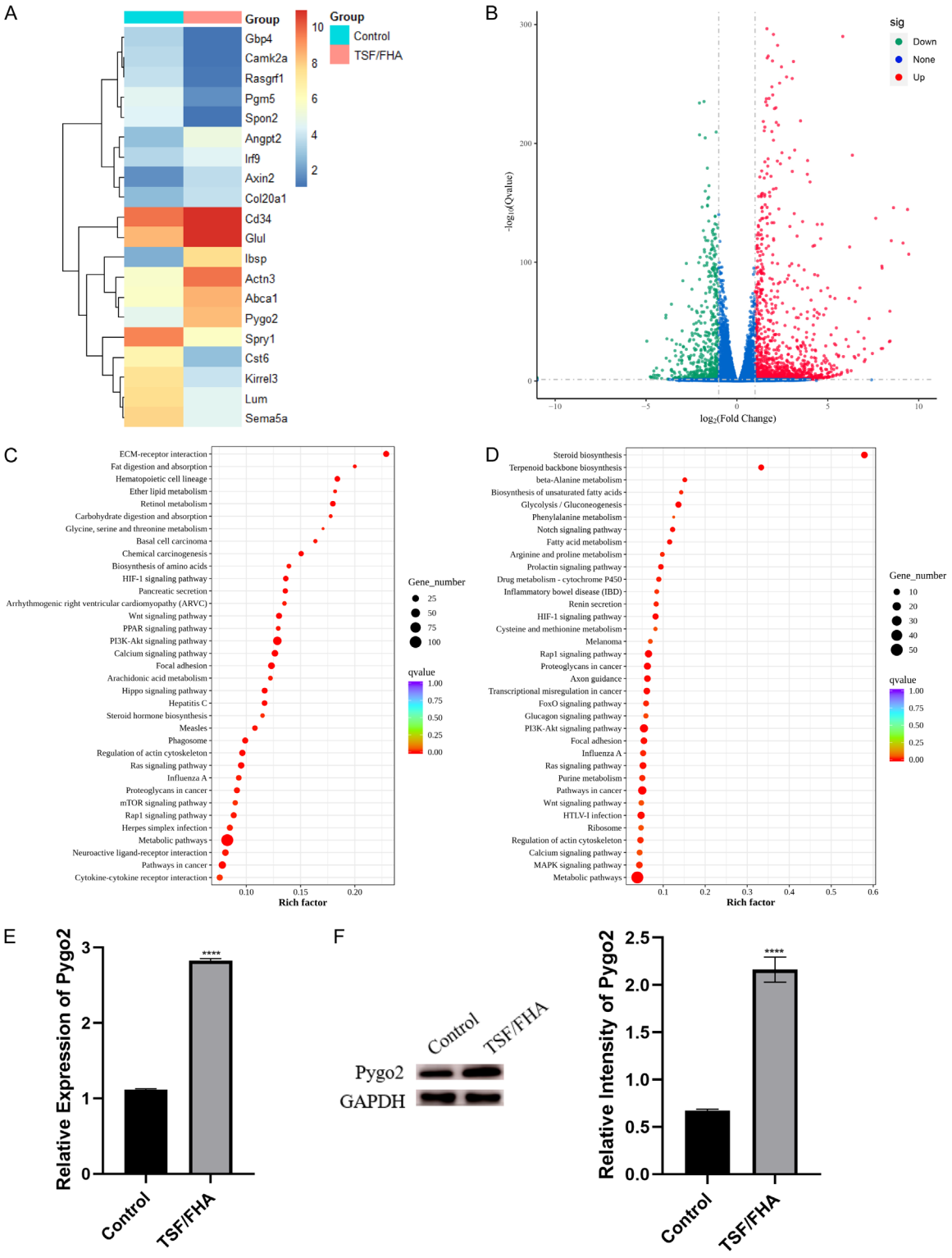

Figure 6. Pygo2 expression in the Mc3t3 cells during TSF/FHA induced osteogenesis. The differentially expressed genes between control cells and TSF/FHA-treated cells are shown in the heat map (A) and volcano plot (B). (C, D) The scatterplots of up-regulated or down-regulated KEGG enrichment pathways. (E, F) The Pyoo2 expression in control group and TSF/FHA-treated cells. Tussah Silk Fibroin (TSF)/Fluoridated Hydroxyapatite (FHA).

Table 2. KEGG analysis of pathways influenced by TSF/FHA

Name	ID	Input number	Background number	P
Calcium signaling pathway	mmu04020	31	182	7.98E-07
Wnt signaling pathway	mmu04310	26	146	3.00E-06
Cell adhesion molecules (CAMs)	mmu04514	21	176	0.002674
Signaling pathways regulating pluripotency of stem cells	mmu04550	18	140	0.002908
Insulin signaling pathway	mmu04910	13	142	0.067491
Basal cell carcinoma	mmu05217	11	55	0.001728
Carbohydrate digestion and absorption	mmu04973	9	45	0.004387
Adherens junction	mmu04520	9	74	0.039471
Fat digestion and absorption	mmu04975	8	40	0.007319

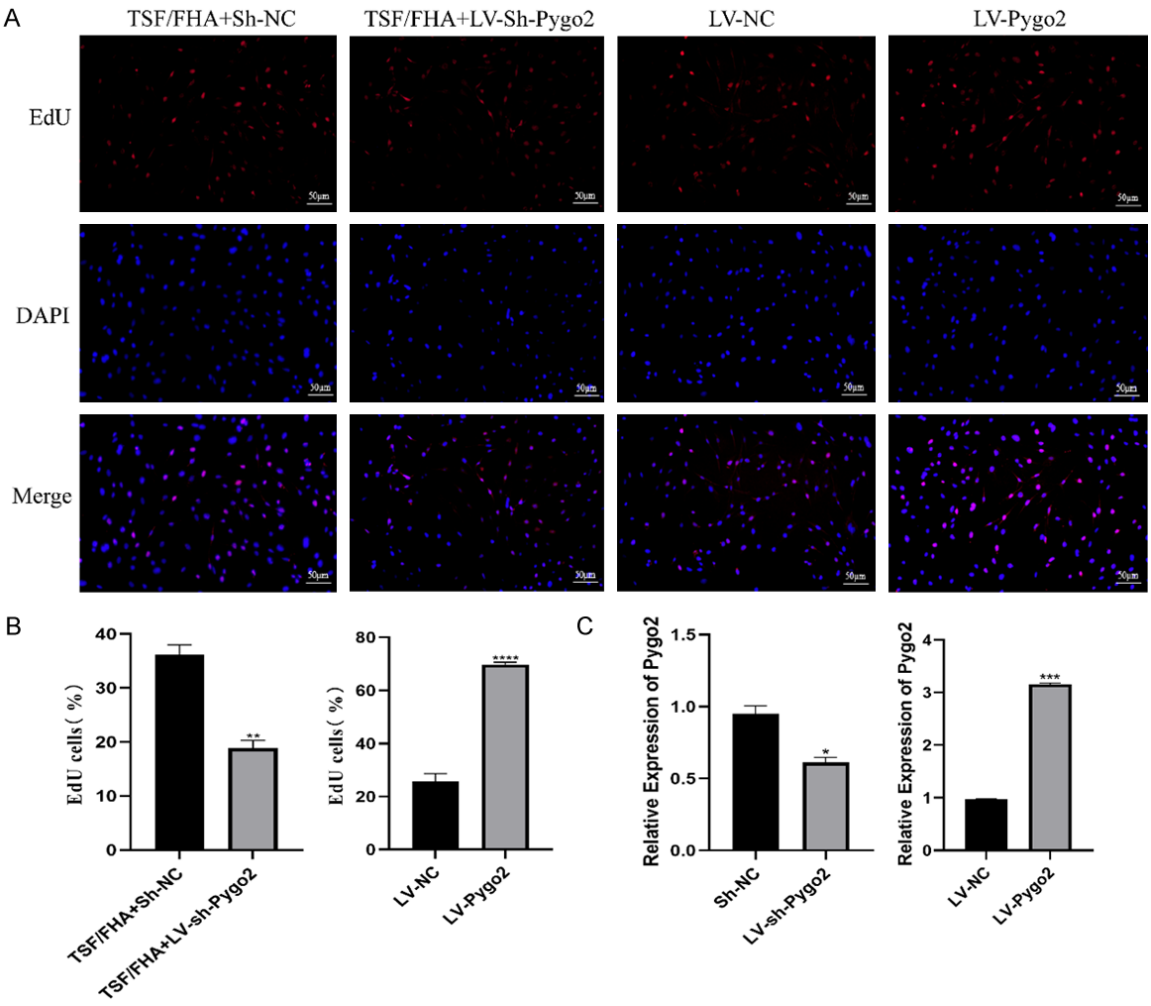

Figure 7. The effect of lentivirus on the proliferation of Mc3t3 cells. A, B. The proliferation of Mc3t3 cells after transfection (EdU staining). C. The transfection efficiency of lentivirus (qRT-PCR). *P<0.05, **P<0.01 *vs* control group. Scale bar, 50 μm.

the LV-sh-Pygo2 group as compared to the Sh-NC group (**Figures 7A**, **7B**, **8A**, **8B**). As shown in **Figure 8C**, when Pygo2 was overexpressed, active β-catenin expression also increased which suggested that Pygo2 overexpression activated the Wnt/β-catenin signaling pathway.

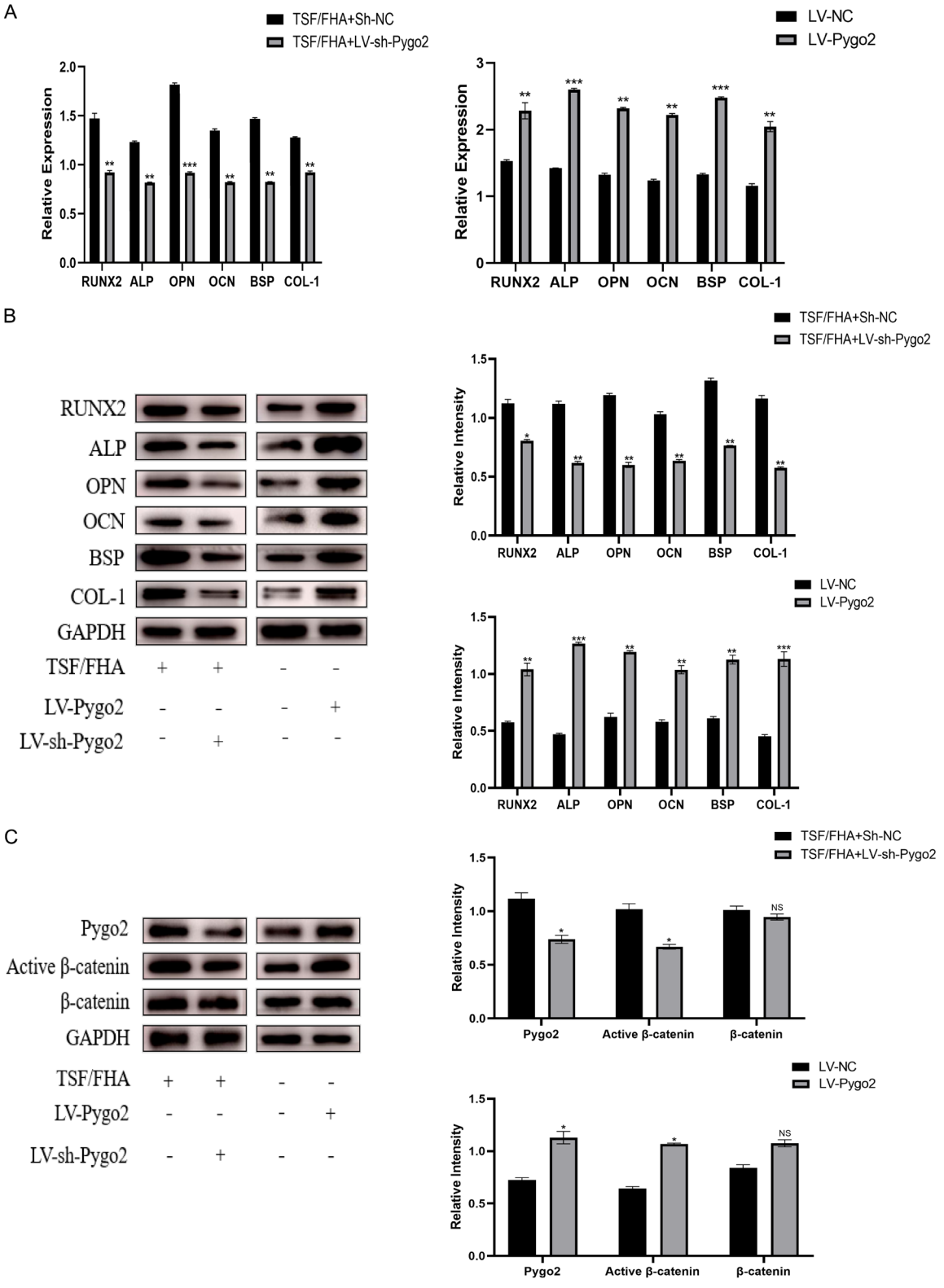

Figure 8. TSF/FHA regulates the osteogenic differentiation of Mc3t3 cells by promoting Pygo2 expression. The expression of osteogenic genes and proteins decreased significantly in the TSF/FHA + LV-sh-Pygo2 group as compared to the TSF/FHA + Sh-NC group as assessed by (A) qRT-PCR and (B) Western blotting. Besides, the expression of osteogenic genes and proteins increased in the LV-Pygo2 group as compared to the LV-NC group. (C) The expression of active β-catenin changed in the LV-Pygo2 group and TSF/FHA + LV-sh-Pygo2 group. *P<0.05, **P<0.01 *vs* control group. Tussah Silk Fibroin (TSF)/Fluoridated Hydroxyapatite (FHA).

Overall, these results indicate that TSF/FHA activates the Wnt/β-catenin signaling pathway by inducing Pygo2 expression, thereby promotes the proliferation and osteogenic differentiation of Mc3t3 cells.

Bone regeneration in the skull defect of SD rats

Mc3t3 cells with or without transfection were grown on the TSF/FHA and then implanted into the skull defect of SD rats. The skulls were harvested after 8 weeks for the evaluation of bone regeneration. Postoperative inflammation was not observed, indicating that TSF/FHA has good biocompatibility. Micro-CT and μCT showed that there was no new bone formed at the defect site in the control group (**Figure 9A**). The density of new bone formed in each experimental group increased significantly as compared to the control group ($P<0.05$), and the TSF/FHA + LV-Pygo2 group had the largest new bone density, bone area and bone mass ($P<0.01$), and the bone was continuous (**Figure 9B**). Newly formed bone was blue on Masson staining (**Figure 10A**). The new bone density, area and bone mass significantly reduced, and the upper and lower bone plates were deformed in the TSF/FHA + LV-sh-Pygo2 group (**Figure 10A**, **10B**). The expression of osteogenesis related proteins (such as RUNX2, ALP, OPN, OCN and BSP) were detected by immunohistology. Results showed high expression of these proteins in the LV-Pygo2 group and low expression in the LV-sh-Pygo2 group (**Figure 10B**). These results suggest that TSF/FHA may regulate osteogenic differentiation of Mc3t3 cells via Pygo2 and TSF/FHA can induce the osteogenic differentiation of Mc3t3 cells.

Discussion

In recent years, the clinical treatment of bone defects caused by cancer, congenital malformation, trauma and surgery has been a challenge, and therefore the development of new methods for the bone reconstruction has been a hot topic in the orthopedic research field [28, 29]. Autologous bone is one of the most ideal replacement materials, but there are still some disadvantages including more trauma, insufficient supply and obvious absorption [30]. Synthetic materials have recently been extensively studied to avoid these disadvantages [31]. Bone tissue engineering (BTE) can simulate organic-inorganic composition of bone tissues by mixing macromolecules as organic matrix and HA as inorganic phase at an appropriate proportion [32].

The concept of electrospinning was first proposed by American Formhals in 1934 [33], and it is currently the only technology in the world that is still employed for the preparation of nanofibers [34, 35]. In this procedure, a high voltage electric field is applied to the SF solution in the syringe by using a high voltage power supply [36]. At the same time, a strong electric field force will be generated between the receiving device and the syringe needle, which makes the SF solution in the needle converge into Taylor cone [37]. Then, an electrostatic jet formed by the SF polymer solution is ejected from the needle and reaches the receiving device to form a nanosilk membrane, which can simulate the structure and function of type I collagen in the natural bone [37]. In addition, TSF film can induce HA to form self-assembled nanocomposite materials on its surface [12, 38]. FHA crystals can be prepared on the surface of teeth and nano-PCL films by phosphate cycling immersion [23, 24]. In this study, TSF film was prepared by electrostatic spinning technology, and then HA and FHA were mixed into the TSF/FHA composite with phosphate cycling immersion method. Thus the TSF/FHA composite could simultaneously simulate the organic and inorganic components in the natural bone.

The compounds of TSF or FHA with other materials have been employed to stimulate bone regeneration of mesenchymal stem cells (MSCs) [39, 40]. Whether the composite of TSF/FHA can promote bone regeneration remains unknown. We evaluated the ability of TSF/FHA to induce osteogenesis and explored the underlying mechanism. To study the fluoride ion substitution of hydroxide radical, a series of fluoride ion substitutions (TSF/F_0HA, TSF/F_1HA, TSF/F_2HA) were tested. The results of SEM, EDS, FTIR and XRD confirmed that HA was deposited on the surface of TSF film, and fluoride ions were also doped into HA to synthesize FHA. The crystallinity of FHA was higher than that of HA, which was consistent with previous findings [16]. All TSF/FHA, especially TSF/F_1HA, were able to promote osteogenic differentiation of Mc3t3 cells. In addition, fluoride ion at an appropriate proportion accelerated the osteogenesis, which was consistent with

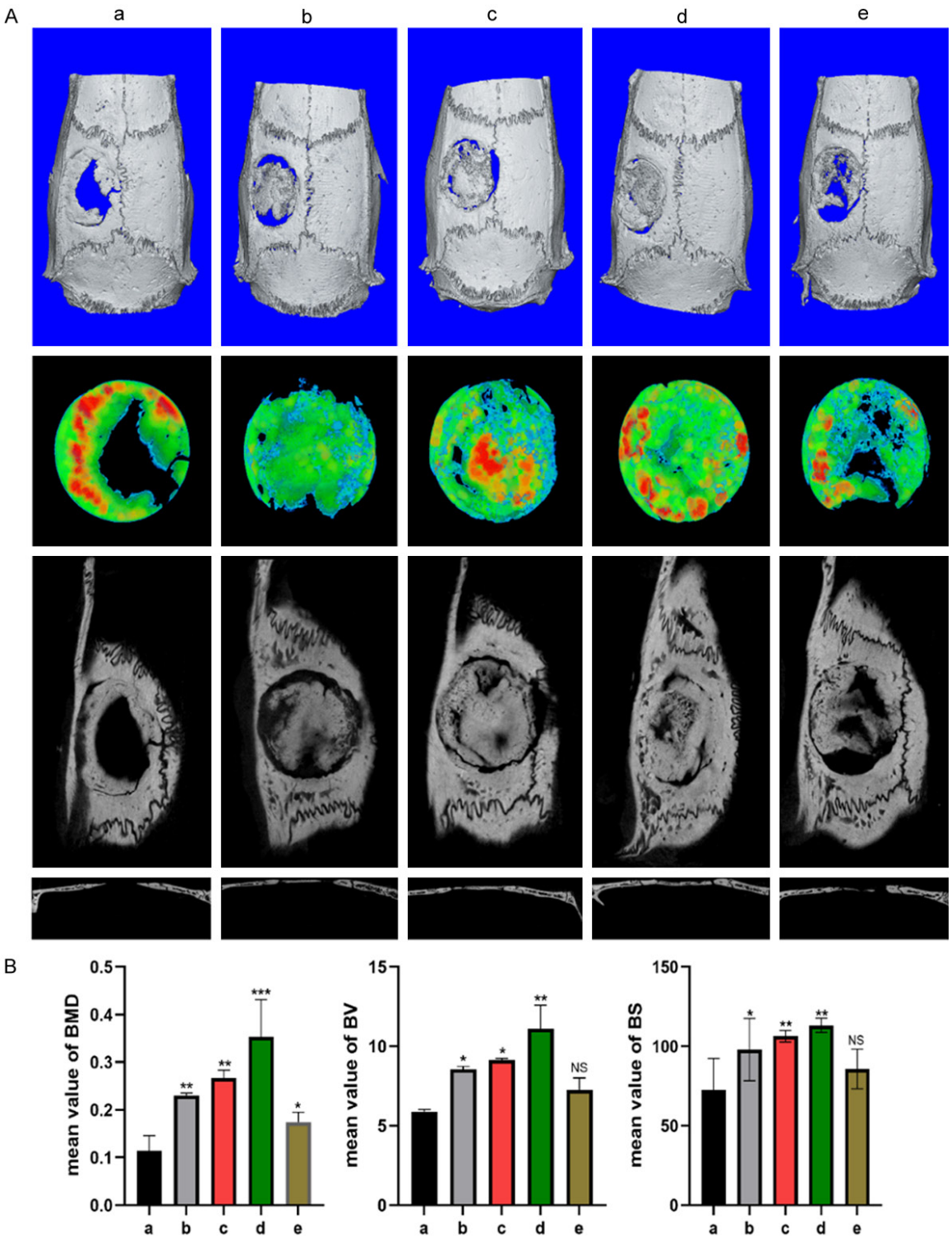

Figure 9. Amounts of regenerated bone in each group. (A) Micro-CT and μCT of regenerated bone in each group. (B) Quantification of regenerated bone in each group. (Aa, Ba) Control group, (Ab, Bb) TSF/FHA group, (Ac, Bc) TSF/FHA + untreated Mc3t3 cells, (Ad, Bd) TSF/FHA + LV-Pygo2 Mc3t3 cells, (Ae, Be) TSF/FHA + LV-sh-Pygo2 Mc3t3 cells. *BMD: Bone Mineral Density, BV: Bone Volume, BS: Bone Surface. Tussah Silk Fibroin (TSF)/Fluoridated Hydroxyapatite (FHA).

previous findings [41, 42]. The TSF/F_1HA was the best to induce the osteogenesis, and thus it was used in the following experiments (TSF/FHA group).

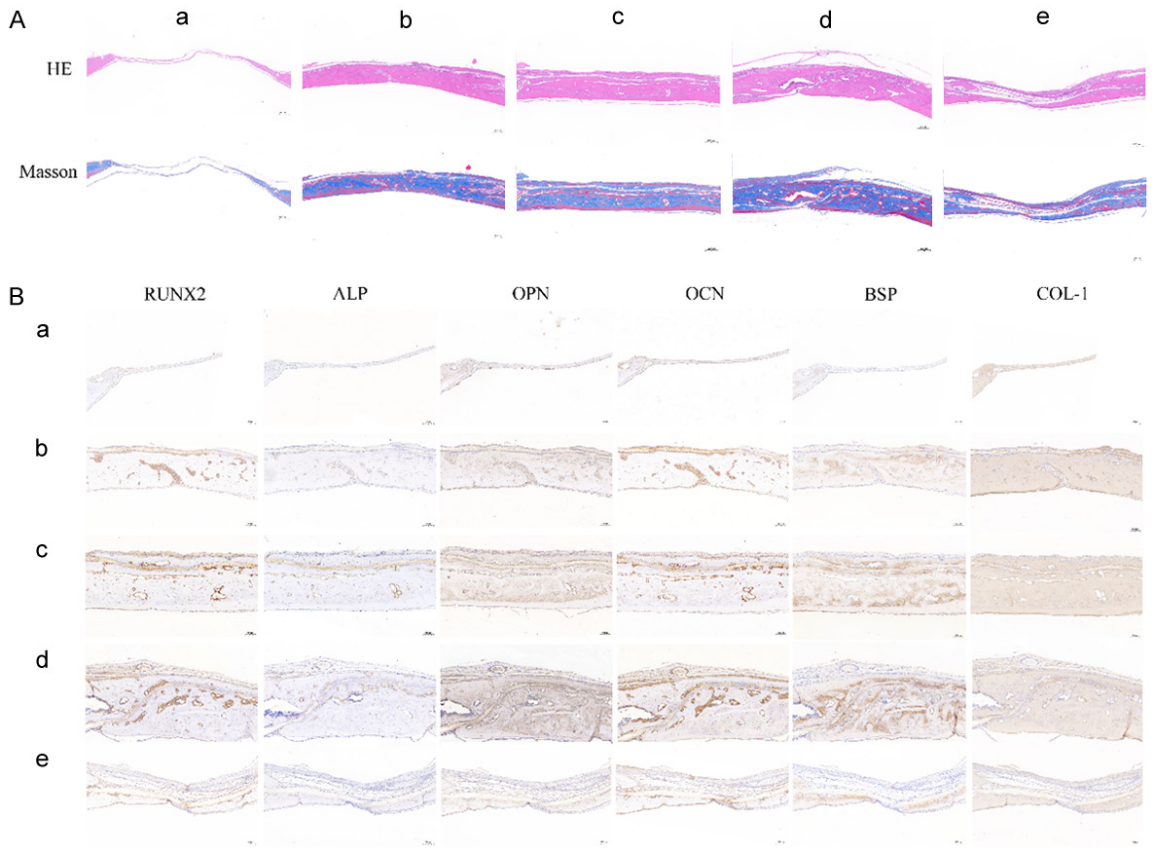

Figure 10. HE staining, Masson staining (A) and immunohistochemical staining (B) of defect bone collected at 8 weeks after cell implantation. Different amounts of regenerated bone formed were observed in each group. (Aa, Ba) Control group, (Ab, Bb) TSF/FHA group, (Ac, Bc) TSF/FHA + untreated Mc3t3 cells, (Ad, Bd) TSF/FHA + LV-Pygo2 Mc3t3 cells, (Ae, Be) TSF/FHA + LV-sh-Pygo2 Mc3t3 cells. Scale bar, 200 μm. Tussah Silk Fibroin (TSF), Fluoridated Hydroxyapatite (FHA).

The mechanism underlying the TSF/FHA induced osteogenic differentiation was further investigated. Axin2 is a responsive gene of the Wnt/β-catenin signaling pathway [43]. Pygo2 directly binds to Legless which then binds to active β-catenin [44]. This improves the combination of active β-catenin [2] with lymphoid enhancement factors and T cell factor (LEF/TCF) [45, 46], thus enhancing the transcription of downstream target genes of Wnt/β-catenin signaling pathway [17, 47] and negatively regulating the adipogenesis [22]. RNA-seq indicated that the canonical Wnt/β-catenin signaling pathway was activated after TSF/FHA induction and the expression of some Wnt-related genes changed including Pygo2 and Axin2 with upregulated expression. In the following experiments, Pygo2 was further investigated. Our results showed the mRNA and protein expression of Pygo2 increased in the TSF/FHA-treated group. Meanwhile, the mRNA and protein expression of active β-catenin increased. These results suggest that TSF/FHA acts through activating the canonical Wnt/β-catenin pathway.

To understand the role of Pygo2 in the TSF/FHA induced osteogenic differentiation of Mc3t3 cells, a lentiviral system was constructed to knockdown or overexpress Pygo2 in Mc3t3 cells. The expression of Pygo2, active β-catenin, and osteogenic genes increased significantly in the LV-Pygo2 group as compared to the LV-NC group. However, in the LV-sh-Pygo2 group with TSF/FHA induction, the expression of Pygo2, active β-catenin, osteogenic genes reduced markedly as compared to the Sh-NC group. Since the increased expression of active β-catenin indicates the activation of Wnt/β-catenin signaling pathway [25], our results emphasized the role of Pygo2 in the Wnt/β-catenin signaling pathway during the osteogenic differentiation of Mc3t3 cells. This result was also confirmed in SD rats with skull defect. In the control group, only a small amount of new

bone was observed at the defect site. HE staining, Masson staining and immunohistochemical staining showed new bone formation in the upper and lower layers of the scaffold materials in remaining 4 groups, and the bone lacunae were obvious on the surface of materials and in the new bone tissues. The material was not completely degraded, and no obvious inflammation was observed around it, indicating that the material had good biocompatibility, low toxicity and precise osteogenic ability.

There are some limitations in this study. The cells used in this study are precursor osteoblasts. Whether TSF/FHA can promote osteogenic differentiation of mesenchymal stem cells and other cells remains to be confirmed. In the animal model, the expression of COL-1 was much lower than that of other non-collagen proteins, indicating that the environment *in vivo* is more complicated than that *in vitro*. Moreover, SD rats were used as the experimental animals in this study. Whether the results in our study are also applicable to larger animals needs to be further studied.

Conclusions

In conclusion, our study indicates that TSF/FHA may accelerate osteogenesis by upregulating Pygo2 and activating the Wnt/β-catenin signaling pathway.

Acknowledgements

This study was supported by the Department of Oral and Maxillofacial Surgery, the First Affiliated Hospital and Academy of Medical Sciences of Zhengzhou University.

Disclosure of conflict of interest

None.

Address correspondence to: Weiliu Qiu, Department of Stomatology, The First Affiliated Hospital of Zhengzhou University, Zhengzhou, Henan, China. E-mail: qiuwl@cae.cn

References

[1] Zhang W, Wang N, Yang M, Sun T, Zhang J, Zhao Y, Huo N and Li Z. Periosteum and development of the tissue-engineered periosteum for guided bone regeneration. J Orthop Translat 2022; 33: 41-54.

[2] Hollý D, Klein M, Mazreku M, Zamborský R, Polák Š, Danišovič Ľ and Csöbönyeiová M. Stem cells and their derivatives-implications for alveolar bone regeneration: a comprehensive review. Int J Mol Sci 2021; 22: 11746.

[3] Cui B, Zhang C, Gan B, Liu W, Liang J, Fan Z, Wen Y, Yang Y, Peng X and Zhou Y. Collagen-tussah silk fibroin hybrid scaffolds loaded with bone mesenchymal stem cells promote skin wound repair in rats. Mater Sci Eng C Mater Biol Appl 2020; 109: 110611.

[4] Singh YP and Dasgupta S. Gelatin-based electrospun and lyophilized scaffolds with nano scale feature for bone tissue engineering application: review. J Biomater Sci Polym Ed 2022; 33: 1704-1758.

[5] Ravichandran R, Venugopal JR, Sundarrajan S, Mukherjee S and Ramakrishna S. Precipitation of nanohydroxyapatite on PLLA/PBLG/Collagen nanofibrous structures for the differentiation of adipose derived stem cells to osteogenic lineage. Biomaterials 2012; 33: 846-855.

[6] Rodríguez-Merchán EC. Bone healing materials in the treatment of recalcitrant nonunions and bone defects. Int J Mol Sci 2022; 23: 3352.

[7] Nosrati H, Sarraf-Mamoory R, Le DQS, Zolfaghari Emameh R, Canillas Perez M and Bünger CE. Improving the mechanical behavior of reduced graphene oxide/hydroxyapatite nanocomposites using gas injection into powders synthesis autoclave. Sci Rep 2020; 10: 8552.

[8] Qasim SB, Zafar MS, Najeeb S, Khurshid Z, Shah AH, Husain S and Rehman IU. Electrospinning of chitosan-based solutions for tissue engineering and regenerative medicine. Int J Mol Sci 2018; 19: 407.

[9] Saleem M, Rasheed S and Yougen C. Silk fibroin/hydroxyapatite scaffold: a highly compatible material for bone regeneration. Sci Technol Adv Mater 2020; 21: 242-266.

[10] Grabska-Zielińska S and Sionkowska A. How to improve physico-chemical properties of silk fibroin materials for biomedical applications?-Blending and cross-linking of silk fibroin-a review. Materials (Basel) 2021; 14: 1510.

[11] Wu J, Cao L, Liu Y, Zheng A, Jiao D, Zeng D, Wang X, Kaplan DL and Jiang X. Functionalization of silk fibroin electrospun scaffolds via BMSC affinity peptide grafting through oxidative self-polymerization of dopamine for bone regeneration. ACS Appl Mater Interfaces 2019; 11: 8878-8895.

[12] Silva SS, Kundu B, Lu S, Reis RL and Kundu SC. Chinese oak tasar silkworm antheraea pernyi silk proteins: current strategies and fu-

ture perspectives for biomedical applications. Macromol Biosci 2019; 19: e1800252.
[13] Wu P, Zhang P, Zheng H, Zuo B, Duan X, Chen J, Wang X and Shen Y. Biological effects different diameters of Tussah silk fibroin nanofibers on olfactory ensheathing cells. Exp Ther Med 2019; 17: 123-130.
[14] Dai C, Li Y, Pan W, Wang G, Huang R, Bu Y, Liao X, Guo K and Gao F. Three-dimensional high-porosity chitosan/honeycomb porous carbon/hydroxyapatite scaffold with enhanced osteoinductivity for bone regeneration. ACS Biomater Sci Eng 2020; 6: 575-586.
[15] Park H, Ryu J, Jung S, Park H, Oh H and Kook M. Effect of hydroxyapatite nanoparticles and nitrogen plasma treatment on osteoblast biological behaviors of 3D-printed HDPE scaffold for bone tissue regeneration applications. Materials (Basel) 2022; 15: 827.
[16] Bolhari B, Sooratgar A, Pourhajibagher M, Chitsaz N and Hamraz I. Evaluation of the antimicrobial effect of mineral trioxide aggregate mixed with fluorohydroxyapatite against E. faecalis in vitro. ScientificWorldJournal 2021; 2021: 6318690.
[17] Czekanska EM, Stoddart MJ, Richards RG and Hayes JS. In search of an osteoblast cell model for in vitro research. Eur Cell Mater 2012; 24: 1-17.
[18] Yamada S, Obata A, Maeda H, Ota Y and Kasuga T. Development of magnesium and siloxane-containing vaterite and its composite materials for bone regeneration. Front Bioeng Biotechnol 2015; 3: 195.
[19] Su Y, Wen J, Zhu J, Xie Z, Liu C, Ma C, Zhang Q, Xu X and Wu X. Pre-aggregation of scalp progenitor dermal and epidermal stem cells activates the WNT pathway and promotes hair follicle formation in in vitro and in vivo systems. Stem Cell Res Ther 2019; 10: 403.
[20] Deng L, Hong H, Zhang X, Chen D, Chen Z, Ling J and Wu L. Down-regulated lncRNA MEG3 promotes osteogenic differentiation of human dental follicle stem cells by epigenetically regulating Wnt pathway. Biochem Biophys Res Commun 2018; 503: 2061-2067.
[21] Cantù C, Pagella P, Shajiei TD, Zimmerli D, Valenta T, Hausmann G, Basler K and Mitsiadis TA. A cytoplasmic role of Wnt/β-catenin transcriptional cofactors Bcl9, Bcl9l, and Pygopus in tooth enamel formation. Sci Signal 2017; 10: eaah4598.
[22] Xie YY, Mo CL, Cai YH, Wang WJ, Hong XX, Zhang KK, Liu QF, Liu YJ, Hong JJ, He T, Zheng ZZ, Mo W and Li BA. Pygo2 regulates adiposity and glucose homeostasis via β-catenin-Axin2-GSK3β signaling pathway. Diabetes 2018; 67: 2569-2584.
[23] Yin Y, Yun S, Fang J and Chen H. Chemical regeneration of human tooth enamel under near-physiological conditions. Chem Commun (Camb) 2009; 5892-5894.
[24] Guo T, Li Y, Cao G, Zhang Z, Chang S, Czajka-Jakubowska A, Nör JE, Clarkson BH and Liu J. Fluorapatite-modified scaffold on dental pulp stem cell mineralization. J Dent Res 2014; 93: 1290-1295.
[25] Liu S, Sun J, Yuan S, Yang Y, Gong Y, Wang Y, Guo R, Zhang X, Liu Y, Mi H, Wang M, Liu M and Li R. Treated dentin matrix induces odontogenic differentiation of dental pulp stem cells via regulation of Wnt/β-catenin signaling. Bioact Mater 2021; 7: 85-97.
[26] Budi HS, Jameel MF, Widjaja G, Alasady MS, Mahmudiono T, Mustafa YF, Fardeeva I and Kuznetsova M. Study on the role of nano antibacterial materials in orthodontics (a review). Braz J Biol 2022; 84: e257070.
[27] Guo XL, Rao QL and Li LL. Preparation of fluoride-hydroxyapatite and study on effects of fluoride. Journal of Chinese Ceramics 2016; 52: 44-48.
[28] Brown A, Zaky S, Ray H Jr and Sfeir C. Porous magnesium/PLGA composite scaffolds for enhanced bone regeneration following tooth extraction. Acta Biomater 2015; 11: 543-553.
[29] Nie H, Lee CH, Tan J, Lu C, Mendelson A, Chen M, Embree MC, Kong K, Shah B, Wang S, Cho S and Mao JJ. Musculoskeletal tissue engineering by endogenous stem/progenitor cells. Cell Tissue Res 2012; 347: 665-676.
[30] Kao ST and Scott DD. A review of bone substitutes. Oral Maxillofac Surg Clin North Am 2007; 19: 513-521, vi.
[31] Archunan MW and Petronis S. Bone grafts in trauma and orthopaedics. Cureus 2021; 13: e17705.
[32] Zhang J, Nie J, Zhang Q, Li Y, Wang Z and Hu Q. Preparation and characterization of bionic bone structure chitosan/hydroxyapatite scaffold for bone tissue engineering. J Biomater Sci Polym Ed 2014; 25: 61-74.
[33] Cai S, Hu G and Ren J. Processing, properties and application of poly lactic acid (PLA) fiber. Sheng Wu Gong Cheng Xue Bao 2016; 32: 786-797.
[34] Wang YW, Zhang X, Wang TR, Jian-Xin HE and Cui SZ. Electrostatic spinning of tussah silk fibroin/chitosan blend system. Journal of Cellulose Science and Technology 2010.
[35] Nobeshima T, Ishii Y, Sakai H, Uemura S and Yoshida M. Actuation behavior of polylactic acid fiber films prepared by electrospinning. J Nanosci Nanotechnol 2016; 16: 3343-3348.
[36] Otoni CG, Queirós MVA, Sabadini JB, Rojas OJ and Loh W. Charge matters: electrostatic complexation as a green approach to assemble advanced functional materials. ACS Omega 2020; 5: 1296-1304.

[37] Rossiter J. Spinning artificial spiderwebs. Sci Robot 2020; 5: eabd0290.
[38] Naskar D, Sapru S, Ghosh AK, Reis RL, Dey T and Kundu SC. Nonmulberry silk proteins: multipurpose ingredient in bio-functional assembly. Biomed Mater 2021; 16.
[39] Gao Y, Shao W, Qian W, He J, Zhou Y, Qi K, Wang L, Cui S and Wang R. Biomineralized poly (l-lactic-co-glycolic acid)-tussah silk fibroin nanofiber fabric with hierarchical architecture as a scaffold for bone tissue engineering. Mater Sci Eng C Mater Biol Appl 2018; 84: 195-207.
[40] Wang SH, Lee SP, Yang CW and Lo CM. Surface modification of biodegradable Mg-based scaffolds for human mesenchymal stem cell proliferation and osteogenic differentiation. Materials (Basel) 2021; 14: 441.
[41] Nasker P, Mukherjee M, Kant S, Tripathy S, Sinha A and Das M. Fluorine substituted nano hydroxyapatite: synthesis, bio-activity and antibacterial response study. Ceramics International 2018; 44: 22008-22013.
[42] Li Z, Huang B, Mai S, Wu X, Zhang H, Qiao W, Luo X and Chen Z. Effects of fluoridation of porcine hydroxyapatite on osteoblastic activity of human MG63 cells. Sci Technol Adv Mater 2015; 16: 035006.
[43] Li S, Wang C, Liu X, Hua S and Liu X. The roles of AXIN2 in tumorigenesis and epigenetic regulation. Fam Cancer 2015; 14: 325-331.
[44] Xue X, Fan C, Wang L, Gao L, Fan K, Peng M, Fang F, Cheng J and Wang J. Ascorbic acid regulates mouse spermatogonial stem cell proliferation in a Wnt/β-catenin/ROS signaling dependent manner. Theriogenology 2022; 184: 61-72.
[45] Monin MB, Krause P, Stelling R, Bocuk D, Niebert S, Klemm F, Pukrop T and Koenig S. The anthelmintic niclosamide inhibits colorectal cancer cell lines via modulation of the canonical and noncanonical Wnt signaling pathway. J Surg Res 2016; 203: 193-205.
[46] Yang Y, Ge Y, Chen G, Yan Z, Yu M, Feng L, Jiang Z, Guo W and Tian W. Hertwig's epithelial root sheath cells regulate osteogenic differentiation of dental follicle cells through the Wnt pathway. Bone 2014; 63: 158-165.
[47] Wend P, Wend K, Krum SA and Miranda-Carboni GA. The role of WNT10B in physiology and disease. Acta Physiol (Oxf) 2012; 204: 34-51.

Supplementary Table 1. Molecular conformation of silk fibroin and wave number range of infrared spectrum (cm^{-1})

conformation	amide I	amide II	amide III	amide IV and others
α helix	1650-1660	1541-1546	1240	600
β fold	1610-1640	1516-1521	1263	700
random coil	1640-1650	1535-1540	1230	650